A

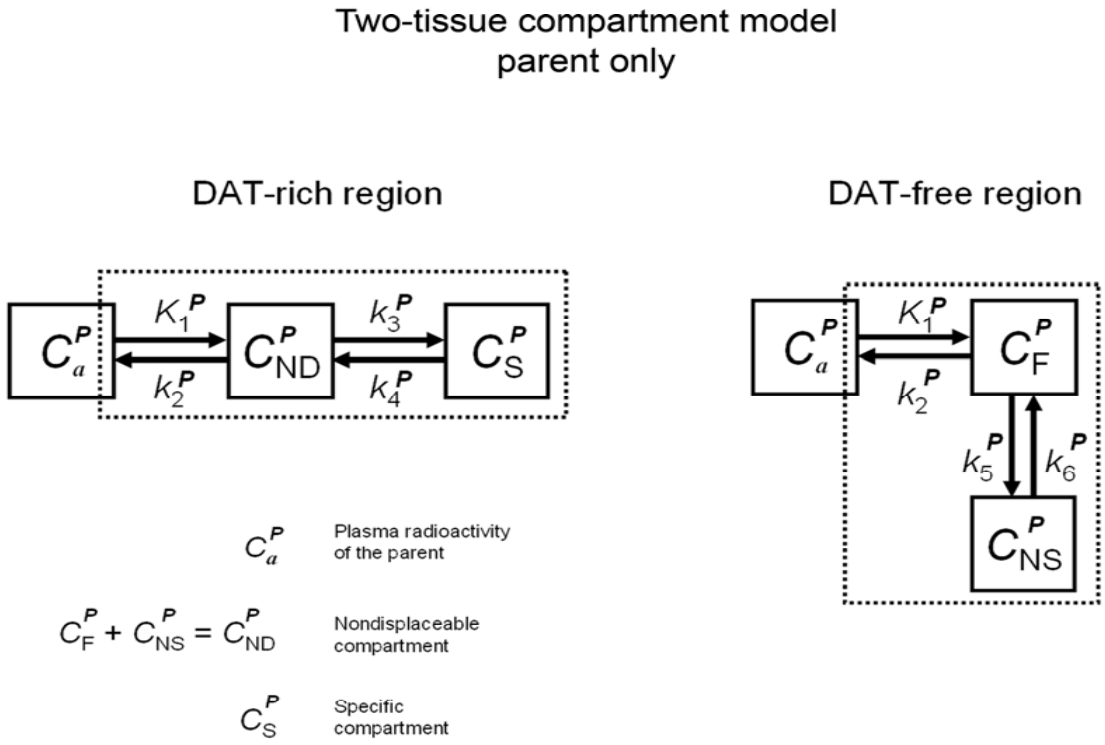
Two-tissue compartment model
parent only
DAT-rich region
DAT-free region
C_a^P
K_1^P
k_2^P
C_{ND}^P
k_3^P
k_4^P
C_S^P
C_F^P
k_5^P
k_6^P
C_{NS}^P
C_a^P Plasma radioactivity of the parent
$C_F^P + C_{NS}^P = C_{ND}^P$ Nondisplaceable compartment
C_S^P Specific compartment

B

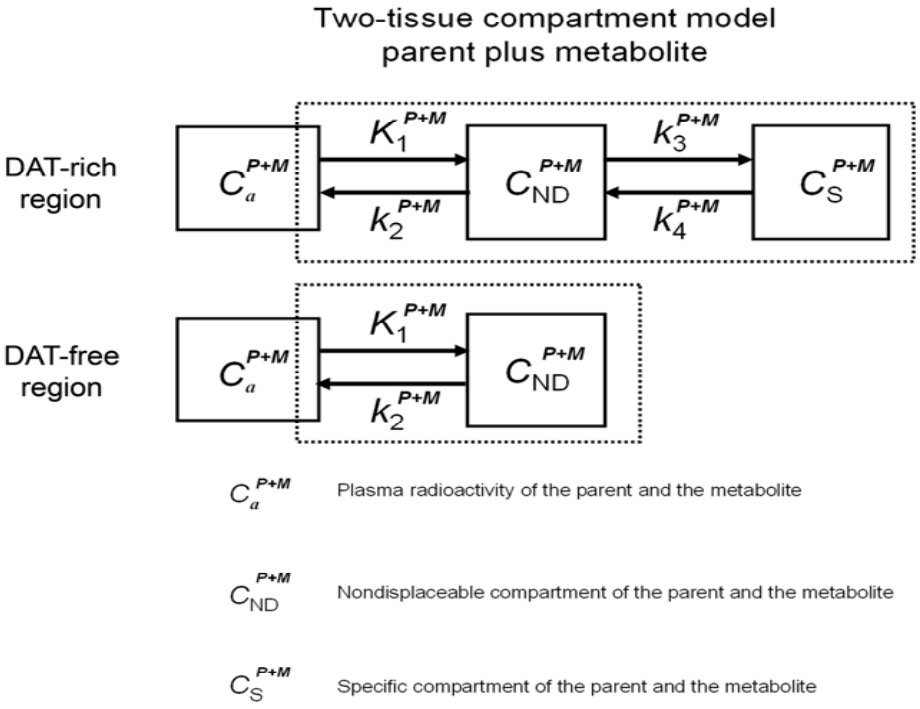
Two-tissue compartment model
parent plus metabolite
DAT-rich region
DAT-free region
C_a^{P+M}
K_1^{P+M}
k_2^{P+M}
C_{ND}^{P+M}
k_3^{P+M}
k_4^{P+M}
C_S^{P+M}
C_a^{P+M} Plasma radioactivity of the parent and the metabolite
C_{ND}^{P+M} Nondisplaceable compartment of the parent and the metabolite
C_S^{P+M} Specific compartment of the parent and the metabolite

Supplemental Figure 1. Two-tissue compartment model with the input function of the parent only (A) or the parent+radiometabolite (B).

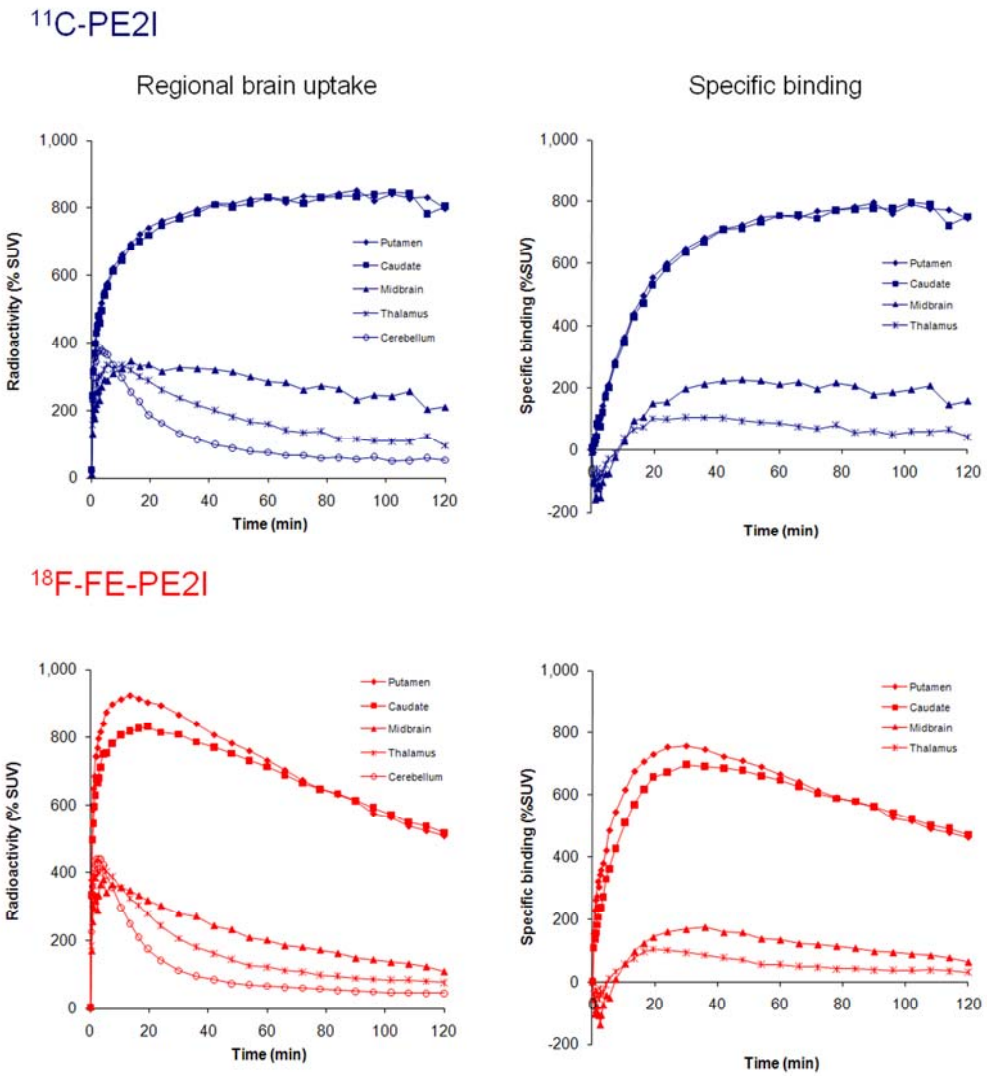
11C-PE2I
Regional brain uptake
Specific binding
Radioactivity (% SUV)
Specific binding (%SUV)
Time (min)
Putamen
Caudate
Midbrain
Thalamus
Cerebellum
18F-FE-PE2I

Supplemental Figure 2. Representative time-activity curves for regional brain uptake and specific binding of [^{11}C]PE2I and [^{18}F]FE-PE2I.

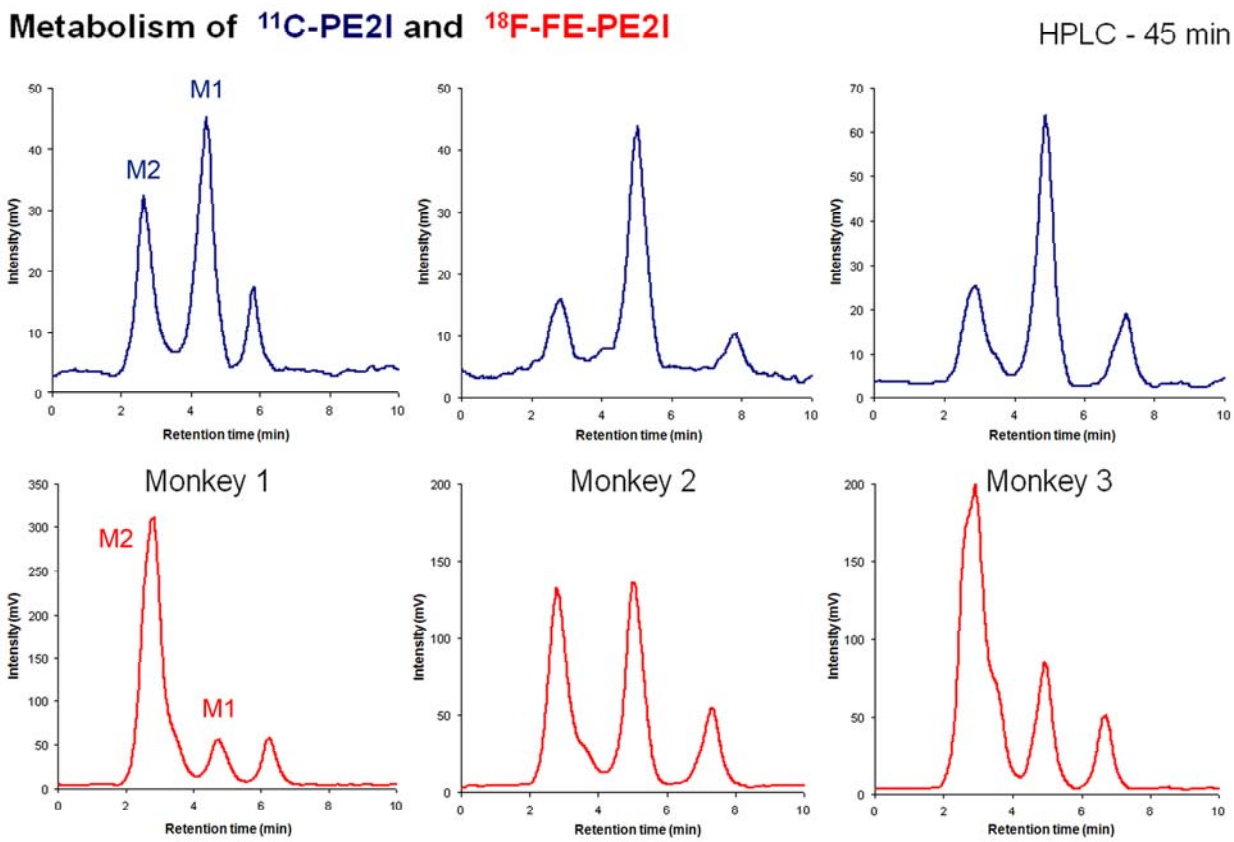
Metabolism of 11C-PE2I and 18F-FE-PE2I
HPLC - 45 min
M1
M2
Intensity (mV)
Retention time (min)
Monkey 1
Monkey 2
Monkey 3
M2
M1

Supplemental Figure 3. HPLC chromatograms at 45 min after injection for [^{11}C]PE2I and [^{18}F]FE-PE2I in all rhesus monkeys examined.

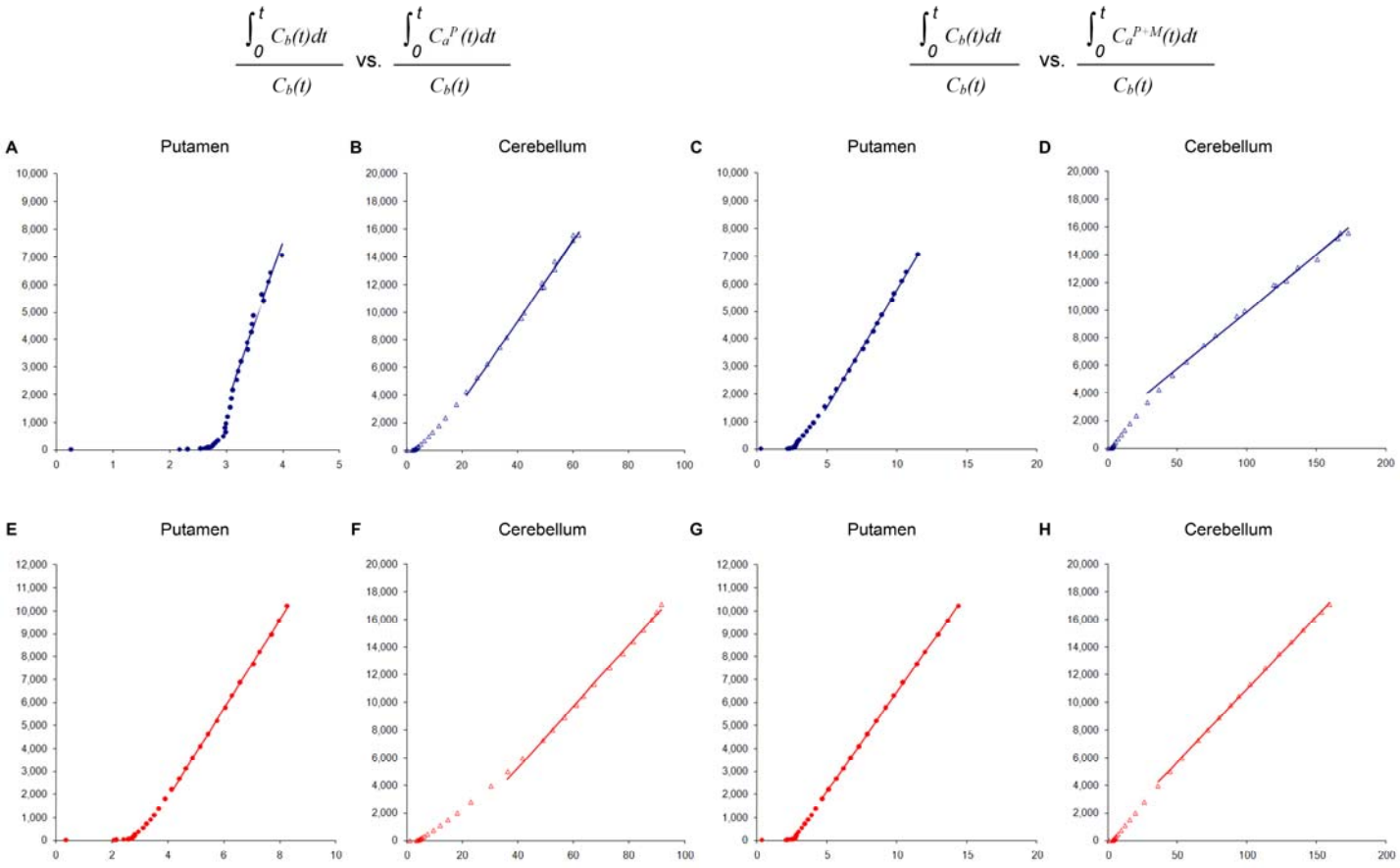
$\frac{\int_0^t C_b(t)dt}{C_b(t)}$ vs. $\frac{\int_0^t C_a^P(t)dt}{C_b(t)}$
$\frac{\int_0^t C_b(t)dt}{C_b(t)}$ vs. $\frac{\int_0^t C_a^{P+M}(t)dt}{C_b(t)}$
A Putamen
B Cerebellum
C Putamen
D Cerebellum
E Putamen
F Cerebellum
G Putamen
H Cerebellum

Supplemental Figure 4. Representative Logan plot with C_a^P input function (Method 3) and graphical analysis plot with the C_a^{P+M} input function (Method 4) of [^{11}C]PE2I (blue, A-D) and [^{18}F]FE-PE2I (red, E-H).

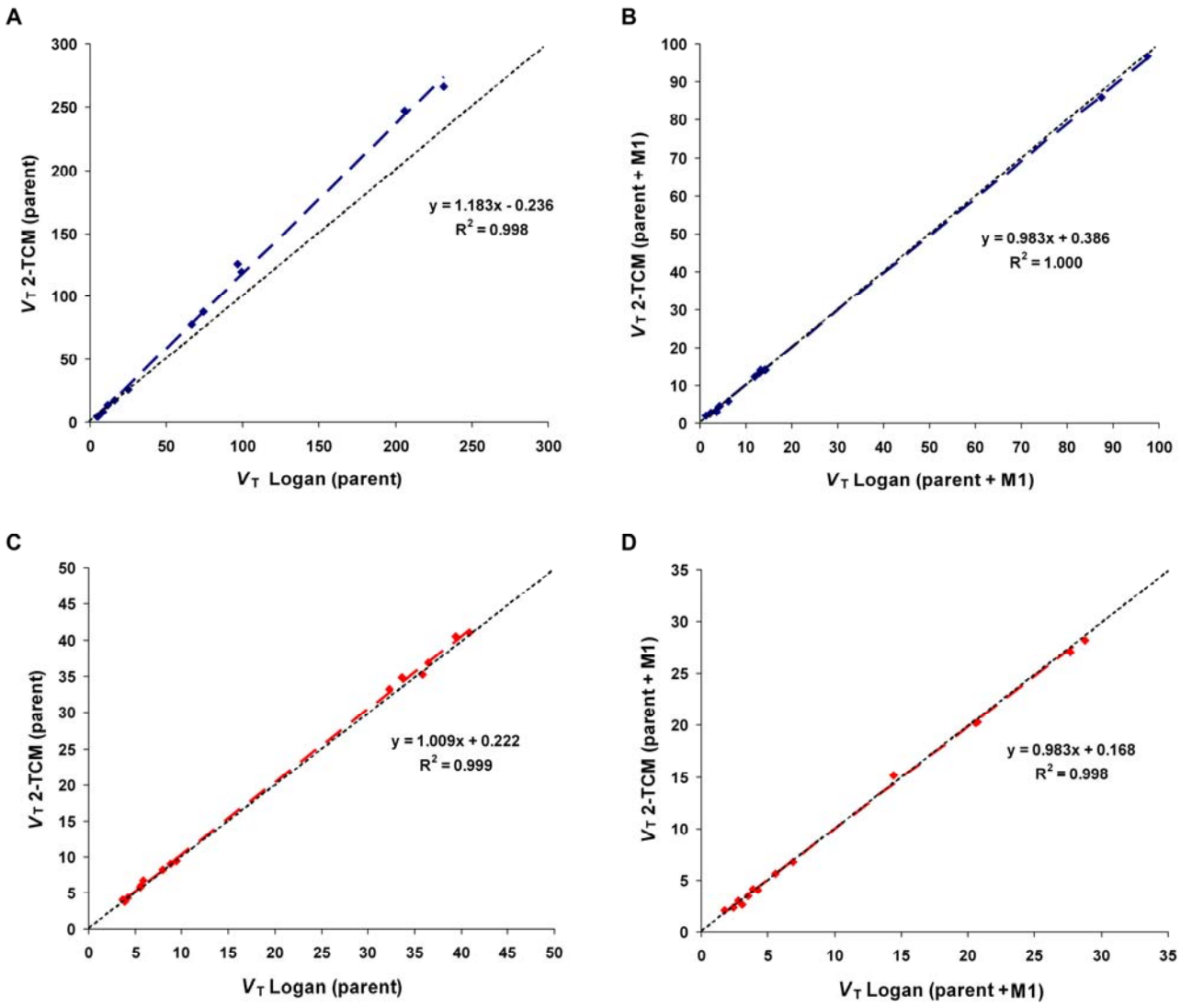
A
V_T 2-TCM (parent)
V_T Logan (parent)
y = 1.183x - 0.236
R^2 = 0.998
B
V_T 2-TCM (parent + M1)
V_T Logan (parent + M1)
y = 0.983x + 0.386
R^2 = 1.000
C
V_T 2-TCM (parent)
V_T Logan (parent)
y = 1.009x + 0.222
R^2 = 0.999
D
V_T 2-TCM (parent + M1)
V_T Logan (parent +M1)
y = 0.983x + 0.168
R^2 = 0.998

Supplemental Figure 5. Correlation between V_T estimated with kinetic analysis (Method 1 or 2) and graphical analysis (Method 3 or 4) for [^{11}C]PE2I (blue, A, B) and [^{18}F]FE-PE2I (red, C, D). Distribution volumes were plotted for all brain regions (caudate, putamen, midbrain, thalamus, and cerebellum).

Supplemental Table 1. Kinetic rate constants estimated with 2-TCM and the input C_a^P (Method 1).

	[^{11}C]PE2I				[^{18}F]FE-PE2I			
	K_1^P	k_2^P	k_3^P	k_4^P	K_1^P	k_2^P	k_3^P	k_4^P
Caudate	0.60±0.13	0.59±0.72	1.04±0.77	0.01±0.00	0.46±0.08	0.11±0.07	0.28±0.12	0.04±0.01
	(6.8±6.1%)	(37.2±36.8%)	(16.7±9.8%)	(21.1±21.1%)	(2.3±1.1%)	(23.9±9.7%)	(23.3±8.6%)	(9.4±1.3%)
Putamen	0.53±0.16	0.16±0.15	0.70±0.45	0.02±0.01	0.49±0.12	0.12±0.11	0.24±0.18	0.04±0.01
	(4.1±3.1%)	(40.0±4.8%)	(27.9±16.8%)	(17.7±3.8%)	(3.1±1.4%)	(26.4±7.5%)	(29.1±10.7%)	(10.1±2.3%)
Midbrain	0.32±0.14	0.08±0.05	0.15±0.05	0.04±0.02	0.22±0.05	0.07±0.02	0.06±0.05	0.03±0.01
	(4.1±1.4%)	(45.7±13.2%)	(70.0±48.1%)	(24.6±17.2%)	(2.0±0.1%)	(15.1±5.0%)	(33.0±12.4%)	(17.7±8.3%)
Thalamus	0.40±0.21	0.08±0.03	0.04±0.07	0.05±0.05	0.26±0.06	0.07±0.01	0.01±0.00	0.01±0.00
	(2.1±1.2%)	(12.9±12.7%)	(40.0±28.3%)	(28.6±9.2%)	(1.5±0.5%)	(5.9±2.4%)	(33.1±15.4%)	(44.3±16.3%)
	K_1^P	k_2^P	k_5^P	k_6^P	K_1^P	k_2^P	k_5^P	k_6^P
Cerebellum	0.49±0.21	0.14±0.03	0.02±0.00	0.03±0.01	0.32±0.09	0.13±0.03	0.01±0.00	0.01±0.01
	(1.8±0.4%)	(6.1±0.5%)	(31.5±7.3%)	(25.8±5.3%)	(1.4±0.4%)	(4.1±1.4%)	(27.5±8.3%)	(40.7±10.6%)

Mean±SD and corresponding %COV of the estimates (mean±SD) in parentheses

Supplemental Table 2. Kinetic rate constants estimated with 2-TCM and the input C_a^{P+M} (Method 2). In the DAT-rich regions K_1^{P+M}/k_2^{P+M} was fixed to the value estimated in the Cerebellum with 1-TCM.

	[^{11}C]PE2I			[^{18}F]FE-PE2I		
	K_1^{P+M}	k_3^{P+M}	k_4^{P+M}	K_1^{P+M}	k_3^{P+M}	k_4^{P+M}
Caudate	0.47±0.03	0.58±0.22	0.08±0.06	0.49±0.09	0.69±0.51	0.10±0.09
	(2.0±0.2%)	(11.5±2.7%)	(13.1±1.2%)	(1.8±1.2%)	(8.0±2.8%)	(8.7±3.2%)
Putamen	0.46±0.03	0.79±0.36	0.12±0.11	0.52±0.10	0.66±0.46	0.09±0.08
	(4.0±1.9%)	(21.3±12.7%)	(22.3±11.6%)	(1.7±1.0%)	(8.7±1.6%)	(9.3±1.3%)
Midbrain	0.26±0.04	1.19±1.24	0.94±1.06	0.22±0.06	0.27±0.33	0.25±0.34
	(3.0±1.2%)	(33.2±38.8%)	(33.9±38.4%)	(1.7±0.2%)	(11.1±2.4%)	(12.1±1.7%)
Thalamus	0.36±0.07	1.20±1.61	3.11±4.17	0.27±0.06	0.29±0.35	0.64±0.80
	(7.3±5.0%)	(21.4±12.2%)	(19.3±11.8%)	(1.7±0.4%)	(17.7±10.4%)	(20.1±11.7%)

Mean±SD and corresponding %COV of the estimates (mean±SD) in parentheses.

Supplemental Appendix A

In this study, the best quantitative approach would be theoretically based on two parallel input functions, one for the parent and one for the metabolite. However, for the reasons already explained (see the Introduction), the model would require 4-tissue compartments and 8 rate constants, which appeared to be rather unstable and provided unreliable estimates of the individual rate constants (data not shown). In an attempt to evaluate the effect of the metabolite on the reference region, the cerebellum was also analyzed with two parallel input functions and a 3-tissue compartment model. Although the model provided a good fit of the data, the identifiability of the individual rate constants was low with %COV above 100-200% in some cases (data not shown).

Supplemental Appendix B
Additional remarks and possible limitations

In this study, kinetic and graphical analyses were performed using the input function of the parent plus the metabolite M1, based on the assumption that only M1 would enter the brain. Based on experimental evidences previously reported in rat (*6*) we believe that such assumption was reasonable and that even if M2 crossed the BBB, its contribution would have been less relevant than M1. In the rat brain M2 is likely converted from M1, since it was found to be present in both striatum and cerebellum (*6*). The conversion of M1 to M2 would require an additional compartment and rate constant for the quantification. However, if M2 was produced from M1 in the rhesus monkey brain, because of its lower lipophilicity, it would have accumulated in the brain. This accumulation seemed to be evident in the rat cerebellum after the injection of [^{11}C]PE2I (see Fig. 2 of (*1*)), but it was not observed in our study for either [^{11}C]PE2I or [^{18}F]FE-PE2I. Therefore, it is reasonable to assume that such conversion was negligible within the time frame of the PET measurements and the rate of conversion of M1 into M2 could be neglected in the compartmental model.

In all three monkeys included this study, because of the different half-lives of the radioisotopes, PET measurements were performed with [^{11}C]PE2I always followed by [^{18}F]FE-PE2I. Under such circumstances, PET measurements with [^{18}F]FE-PE2I were performed after a prolonged anesthesia and this could have an impact on the metabolism of the radioligand. In our previous study (*7*) in cynomolgus monkeys examined with a different type of anesthesia (ketamine+xylazine instead of sevoflurane) and under a shorter time of anesthesia (~1 h instead of ~3-4 h) before the radioligand injection, we observed the same type of metabolism of [^{18}F]FE-PE2I. Therefore, we believe that the

length of anesthesia was not a major contributor of the difference in metabolism observed between [^{11}C]PE2I and [^{18}F]FE-PE2I.

Finally, a possible limitation of the study was that quantification was performed using the total radioactivity concentration of the parent and metabolite in plasma, without the measurement of the free fraction, f_P. Protein binding of radioligands does influence their pharmacokinetic properties and may account for differences in quantitative outcome measures. In this study f_P was not measured and it is not possible to rule out that some of the differences between the two radioligands could be related to differences in protein binding. However, we believe that the differences observed between [^{11}C]PE2I and [^{18}F]FE-PE2I were less likely due to differences in protein binding. The two radioligands showed similar concentration in plasma and similar initial whole brain uptake, suggesting that they have similar BBB penetration, and that the amount of tracer able to freely diffuse from plasma to brain is similar. In addition, the main difference between the two radioligands was indeed the faster wash-out of [^{18}F]FE-PE2I, which is less likely to be related to a difference in f_P and more likely to be related to a difference in k_4 or in vivo affinity for the DAT.

Reference

<jrn>1. Shetty HU, Zoghbi SS, Liow JS, et al. Identification and regional distribution in rat brain of radiometabolites of the dopamine transporter PET radioligand [^{11}C]PE2I. *Eur J Nucl Med Mol Imaging*. 2007;34:667–678.